The Astrophysical Journal, 864:27 (9pp), 2018 September 1 https://doi.org/10.3847/1538-4357/aac726

A Mid-IR Selected Changing-look Quasar and Physical Scenarios for Abrupt AGN Fading

Daniel Stern[1], Barry McKernan[2,3,4], Matthew J. Graham[5], K. E. S. Ford[2,3,4], Nicholas P. Ross[6], Aaron M. Meisner[7,8], Roberto J. Assef[9], Mislav Baloković[5,10], Murray Brightman[5], Arjun Dey[11], Andrew Drake[5], S. G. Djorgovski[5], Peter Eisenhardt[1], and Hyunsung D. Jun[12]

[1] Jet Propulsion Laboratory, California Institute of Technology, 4800 Oak Grove Drive, Mail Stop 169-221, Pasadena, CA 91109, USA; daniel.k.stern@jpl.nasa.gov
[2] Department of Science, Borough of Manhattan Community College, City University of New York, New York, NY 10007, USA
[3] Department of Astrophysics, American Museum of Natural History, New York, NY 10024, USA
[4] Graduate Center, City University of New York, 365 5th Avenue, New York, NY 10016, USA
[5] Cahill Center for Astronomy and Astrophysics, California Institute of Technology, 1216 E. California Boulevard, Pasadena, CA 91125, USA
[6] Institute for Astronomy, SUPA, University of Edinburgh, Royal Observatory, Edinburgh EH9 3HJ, UK
[7] Berkeley Center for Cosmological Physics, Berkeley, CA 94720, USA
[8] Lawrence Berkeley National Laboratory, Berkeley, CA, 94720, USA
[9] Núcleo de Astronomía de la Facultad de Ingeniería y Ciencias, Universidad Diego Portales, Av. Ejército Libertador 441, Santiago, Chile
[10] Harvard-Smithsonian Center for Astrophysics, 60 Garden Street, Cambridge, MA 02138, USA
[11] National Optical Astronomy Observatory, 950 N. Cherry Avenue, Tucson, AZ 85719, USA
[12] School of Physics, Korea Institute for Advanced Study, 85 Hoegiro, Dongdaemun-gu, Seoul 02455, Republic of Korea
Received 2018 March 5; revised 2018 May 17; accepted 2018 May 20; published 2018 August 27

Abstract

We report a new changing-look quasar, WISE J105203.55+151929.5 at $z = 0.303$, found by identifying highly mid-IR-variable quasars in the *Wide-field Infrared Survey Explorer* (*WISE*)/Near-Earth Object WISE Reactivation (NEOWISE) data stream. Compared to multiepoch mid-IR photometry of a large sample of SDSS-confirmed quasars, WISE J1052+1519 is an extreme photometric outlier, fading by more than a factor of two at 3.4 and 4.6 μm since 2009. *Swift* target-of-opportunity observations in 2017 show even stronger fading in the soft X-rays compared to the *ROSAT* detection of this source in 1995, with at least a factor of 15 decrease. We obtained second-epoch spectroscopy with the Palomar telescope in 2017 that, when compared with the 2006 archival SDSS spectrum, reveals that the broad Hβ emission has vanished and that the quasar has become significantly redder. The two most likely interpretations for this dramatic change are source fading or obscuration, where the latter is strongly disfavored by the mid-IR data. We discuss various physical scenarios that could cause such changes in the quasar luminosity over this timescale, and favor changes in the innermost regions of the accretion disk that occur on the thermal and heating/cooling front timescales. We discuss possible physical triggers that could cause these changes, and predict the multiwavelength signatures that could distinguish these physical scenarios.

Key words: galaxies: active – quasars: individual (WISE J105203.55+151929.5)

1. Introduction

While variability has long been recognized as a distinguishing feature of quasars (e.g., Matthews & Sandage 1963), it has only been in recent years that new generations of wide-area, multiepoch optical surveys have allowed systematic study of the extremes of such behavior. In addition to observing such rare phenomena as periodic quasars (e.g., Graham et al. 2015a, 2015b; Liu et al. 2015), flaring quasars (e.g., Lawrence et al. 2016; Graham et al. 2017; Kankare et al. 2017), extreme broad absorption line variability (e.g., Rafiee et al. 2016; Stern et al. 2017), and tidal disruption events (e.g., Arcavi et al. 2014; Blagorodnova et al. 2017), this work has also identified a new class of "changing-look quasars" in which the strong UV continuum and broad hydrogen emission lines associated with unobscured quasars either appear or disappear on timescales of years (e.g., LaMassa et al. 2015; Macleod et al. 2016; Ruan et al. 2016a, 2016b; Runnoe et al. 2016; Gezari et al. 2017; Yang et al. 2018). The physical processes responsible for these changing-look quasars are still debated, but physical changes in the accretion disk structure appear to be the more likely cause rather than changes in obscuration. These disk structural changes are presumed to be associated with changes in the black hole accretion rate.

Related changing-look phenomena have been seen in Seyfert galaxies at lower luminosities for several decades, generally from multiepoch targeted studies of specific sources at either X-ray or optical wavelengths (e.g., Tohline & Osterbrock 1976; Goodrich 1989; Storchi-Bergmann et al. 1995; Shappee et al. 2014, and references therein). Indeed, the term "changing-look" was initially used to describe sources whose X-ray spectra changed appearance on timescales of years, switching from reflection-dominated to Compton-thin, or vice versa (e.g., Matt et al. 2003). In some cases, such as the nearby Seyfert galaxies NGC 1365 and IC 751, the extreme X-ray variability is clearly associated with rapid changes in the nuclear obscuration (e.g., Risaliti et al. 2002; Walton et al. 2014; Rivers et al. 2015; Ricci et al. 2016). On the other hand, Matt et al. (2003) argue that extreme X-ray spectral changes are more typically associated with a temporary switching-off of the nuclear radiation. As one example, McElroy et al. (2016) and Husemann et al. (2016) discuss the case of Mrk 1018 that, over the past four decades, has evolved from a Seyfert 1.9 galaxy to a Seyfert 1 galaxy and then back to a Seyfert 1.9 galaxy. Due to the lack of associated changes in either the Balmer decrement or neutral hydrogen absorbing column of this source, these companion papers argue that intrinsic changes in the accretion disk flux

rather than variable extinction likely drove the spectral evolution of Mrk 1018.

Mid-IR monitoring provides a powerful new tool for both finding changing-look quasars, and for probing the physical processes responsible for the observed changes. X-rays and UV continuum emission from quasars come from regions extremely close to the central supermassive black hole, with separations of a few to a few tens of gravitational radii, $r_g \equiv GM_{\rm BH}/c^2$. This corresponds to distances of less than a light day for typical quasars, and, as long discussed in the context of the unified model of active galactic nuclei (AGNs), the sight line of the observer to this compact region strongly impacts the observed appearance of a quasar at UV and higher energies (e.g., Urry & Padovani 1995). In contrast, the mid-IR emission of quasars predominantly comes from a dusty region beyond the dust sublimation radius, implying parsec-scale distances. Since this larger-scale material, generally believed to be toroidal in structure, is reprocessing emission from the active nucleus, it is both less sensitive to the observer's exact sight line (e.g., Stern et al. 2005, 2012; Assef et al. 2013), and is subject to a substantial time delay relative to luminosity changes in the nuclear regions (e.g., Jun et al. 2015b; Ichikawa & Tazaki 2017).

The *Wide-field Infrared Survey Explorer* (*WISE*; Wright et al. 2010) mission and its continuation as the Near-Earth Object WISE Reactivation (NEOWISE; Mainzer et al. 2014) mission provide ideal data for identifying mid-IR selected changing-look quasars. Since 2010 January, the polar-orbit *WISE* satellite has imaged the full sky approximately every six months. Assef et al. (2018a) presents a catalog of *WISE*-selected AGNs across most of the extragalactic sky, with 4.5 million AGN candidates identified at 90% reliability, and nearly 21 million AGN candidates identified at 75% completeness (but 51% reliability). As part of that work, Assef et al. (2018a) discuss the subset of 687 high-reliability AGNs identified as highly mid-IR variable during the first year of *WISE* observations. Considering the subset of these sources not detected at radio energies, so as to avoid blazars, they present one quasar, WISEA J142846.71+172353.1, whose broad Hα emission has disappeared between an SDSS spectrum obtained in 2008 and a Palomar spectrum obtained in 2017. Assef et al. (2018b) discuss another extreme mid-IR-variable quasar identified from the first year of *WISE* data. Sheng et al. (2017) considers 10 published changing-look AGNs and investigates their mid-IR light curves in the *WISE* and NEOWISE data. They find strong (>0.4 mag) variability in all 10 cases, and they find the mid-IR variability to be consistent with echoing the optical variability with the time lag expected for dust reprocessing. Sheng et al. (2017) argue that this result is inconsistent with varying obscuration causing the changing-look phenomenon, and they instead favor a scenario with variable AGN accretion rates causing the photometric variability.

Here and in a companion paper, Ross et al. (2018), we present the first changing-look quasars identified from the combined *WISE* and NEOWISE data streams. This provides a longer selection baseline than the sample of sources discussed in Assef et al. (2018), which is the only other published example of a mid-IR selected changing-look quasar. Our paper is organized as follows: Section 2 presents the selection of WISE J105203.55+151929.5 (hereafter WISE J1052+1519), which is the focus of this paper. Section 3 presents follow-up spectroscopic observations at optical and X-ray energies, demonstrating the extreme changes in this source. Section 4 presents a detailed discussion of the possible physics that could explain abrupt fading (or brightening) of a quasar; and we summarize our conclusions in Section 5.

Throughout this paper, we use AB magnitudes unless otherwise indicated and we adopt the concordance cosmology, $\Omega_{\rm M} = 0.3$, $\Omega_\Lambda = 0.7$, and $H_0 = 70$ km s^{-1} Mpc^{-1}.

2. Selection of WISE J1052+1519

We extracted mid-IR *W*1 (3.4 μm) and *W*2 (4.6 μm) light curves for ~200,000 Sloan Digital Sky Survey (SDSS) spectroscopic quasars from Data Release 3 (DR3) of the Dark Energy Camera Legacy Survey (DECaLS[13]). These light curves span the period from the beginning of the *WISE* mission in 2010 January through 2014 December, corresponding to the first year of NEOWISE operations. Note that there is a gap in the *WISE* data between 2011 February and 2013 September when the satellite was in hibernation. For most celestial locations, the 90 minute orbit of *WISE* provides ≈12 observations of a source over a ≈1 day period, and a given celestial location is observed every six months. For this study, we combine the shorter-cadence data, and we call each longer cadence coadded observation a single "epoch" of observations. This means that we typically have four epochs of photometry available, with separations ranging from six months to a maximum of nearly five years. The *W*1/*W*2 light curves were obtained by performing forced photometry at the locations of DECam-detected optical sources on un*WISE* epochal coadds (Lang 2014; Lang et al. 2016). While this approach means that we cannot probe variability on timescales of less than 1 day, the coadds allow photometry 1.4 mag deeper than the individual exposures and remove virtually all single-exposure artifacts (e.g., cosmic rays and satellites).

Approximately 30,000 of the SDSS quasars with such *W*1/*W*2 light curves available are "IR-bright," in the sense that they are above both the *W*1 and *W*2 single-exposure thresholds and therefore detected at very high significance in our coadds. For this ensemble of objects, the typical variation in each quasar's measured ($|W1 - W2|$) color is 0.06 magnitudes, which includes statistical and systematic errors. Figure 1 presents the maximum observed mid-IR variability of quasars over the five years of observations, considering only those quasars detected with mean signal-to-noise ratios > 10 in the individual epochs. Most quasars vary by less than 0.2 mag, with a small fraction varying by more than a factor of two in flux over this 4 year period (i.e., $\Delta m \geqslant 0.75$ mag).

To identify the most extreme outliers relative to these trends, we selected objects with the following characteristics:

1. monotonic variation in both *W*1 and *W*2;
2. *W*1 versus *W*2 flux correlation coefficient >0.9; and
3. >0.5 mag peak-to-peak variation in either *W*1 or *W*2.

This yielded a sample of 248 sources, of which 31 are assumed to be blazars due to the presence of radio counterparts in the Faint Images of the Radio Sky at Twenty cm survey (FIRST; Becker et al. 1995). Another 22 are outside the FIRST footprint, leaving 195 radio-undetected ($S_{1.4\rm GHz} \lesssim 1$ mJy; 5σ) quasars in our IR-variable sample. Note that we did not impose our IR-bright criterion in selecting this sample. Doing so in

[13] legacysurvey.org/decamls/

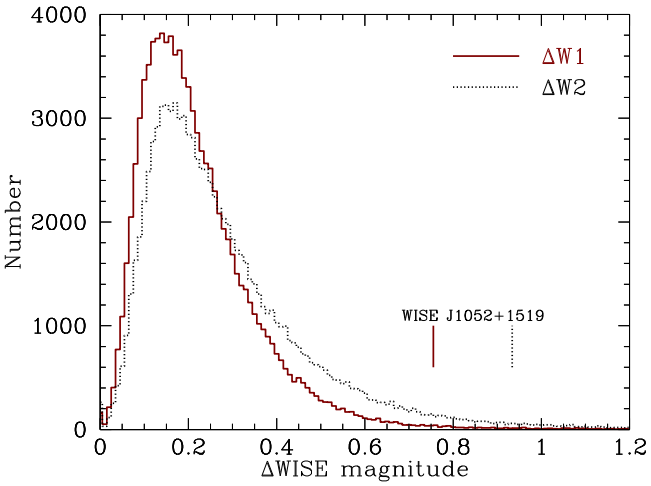

Figure 1. Histogram of maximum variation in mid-IR magnitude between 2010 January and 2014 December for 200,622 quasars in the DECaLS DR3 region. We only plot sources with mean epochal signal-to-noise ratios >10 for each band. WISE J1052+1519 stands out as being highly variable in both *W*1 and *W*2.

future explorations would further cull the sample, potentially allowing us to loosen or remove the monotonicity and correlation coefficient requirements and thereby capture a richer variety of light-curve behaviors. We selected five of these objects for follow-up spectroscopy with Palomar on the night of UT 2017 January 30. WISE J1052+1519, one of these five, had a peak-to-peak variation of 0.76 (0.93) mags in *W*1 (*W*2) between 2010 May and 2014 December, and thus became 0.15 mags bluer in ($W1 - W2$). This made it a significant outlier in both single-band and IR color variability.

2.1. UV to Mid-IR Photometry and Light Curve

Figure 2 presents a multiwavelength light curve of WISE J1052+1519, including optical data from SDSS, the Panoramic Survey Telescope and Rapid Response System (Pan-STARRS; Chambers et al. 2016), DECaLS, and the Catalina Real-time Transient Survey (CRTS; Drake et al. 2009), as well as the mid-IR photometry discussed above. We have also supplemented the $W1/W2$ light curves discussed above with NEOWISE epochal coadds between 2015 May and December, providing two additional mid-IR photometric epochs to the light curve in Figure 2.

Overall, WISE J1052+1519 has faded significantly in the past decade at both optical and mid-IR wavelengths. Optically, the source has changed most at the bluest wavelengths, fading by 1.8 mag at *g*-band between SDSS and DeCaLS, though only by 1.0 mag at *r*-band and 0.8 mag at *z*-band. Figure 3 demonstrates this chromatic change, showing side-by-side false-color optical images from SDSS (2005) and DECaLS (2016): compared to other sources in the field, WISE J1052+1519 has become significantly redder at optical wavelengths over the past decade. In the IR, the situation is reversed, with the more significant fading occurring in the redder *W*2 band, by 0.9 mag, while the bluer *W*1 band faded by only 0.7 mag. Since the spectra of galaxies with ages above a few megayears peak in the near-IR, while AGN spectra peak in the UV and mid-IR, with a dip around 1 μm (e.g., Assef et al. 2010), AGNs become most evident in the rest-frame UV and longwards of a few microns. The observed photometric evolution of WISE J1052+1519 is therefore consistent with a dramatic

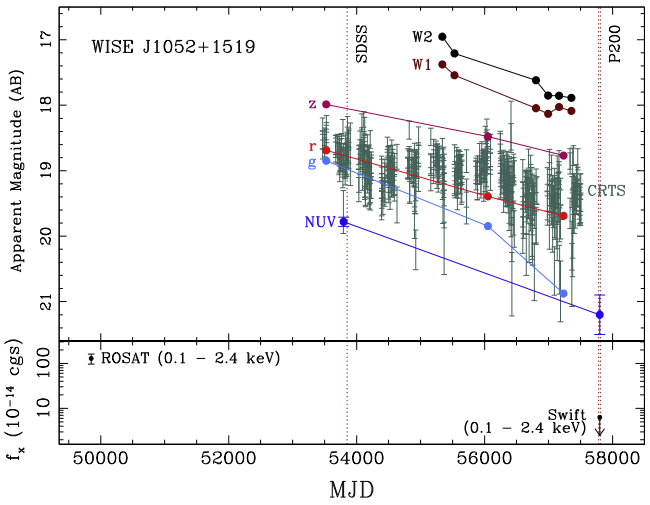

Figure 2. Multiwavelength light curves of WISE J1052+1519, showing the epochs of the spectroscopy with vertical dotted lines. CRTS photometry (green error bars) is unfiltered CCD observations (for details, see Drake et al. 2009). In chronological order, the optical *grz* photometry is from SDSS, Pan-STARRS, and DECaLS. NUV photometry is *GALEX* NUV ($\lambda_{\rm eff} = 2271$ Å) for the first epoch and *Swift*/UVOT UVM2 ($\lambda_{\rm eff} = 2231$ Å) for the second epoch. The bottom panel shows the 0.1–2.4 keV X-ray light curve, where the *ROSAT* point corresponds to the detection in 1995, and the *Swift* point corresponds to the 3σ upper limit for $\Gamma = 2$. WISE J1052+1519 has faded by more than a factor of 15 in the X-rays between the *ROSAT* and *Swift* observations.

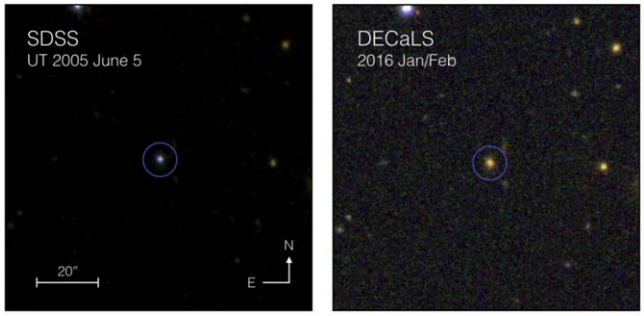

Figure 3. False-color optical images of WISE J1052+1519 from SDSS in 2005 (left) and DECaLS in 2016 (right). In the earlier epoch image, WISE J1052+1519 has a color similar to the blue star to the NNE, while a decade later, the source is considerably redder, comparable in color to the galaxies to the NW.

decrease in its AGN emission. Notably, SDSS morphologically classifies WISE J1052+1519 as stellar, while DECaLS classified the source as "D," meaning a nonstellar source best fit with a de Vaucouleurs profile.

3. Follow-up Observations

3.1. Optical Spectroscopy

WISE J1052+1519 was first observed spectroscopically by SDSS on UT 2006 April 27 (MJD = 53852). The spectrum, shown in Figure 4, reveals a typical quasar with broadened emission lines from multiple hydrogen Balmer transitions (i.e., Hα through Hδ), strong, narrow emission from the [O II] and [O III] doublets, and strong blue continuum rising below ~5500 Å. SDSS reports a redshift of $z = 0.303$ for the source, and classifies it as a quasar.

Because of its unusual light curve, we obtained additional optical spectroscopy of WISE J1052+1519 using the Double Spectrograph (DBSP) on the Hale 200″ Telescope at the

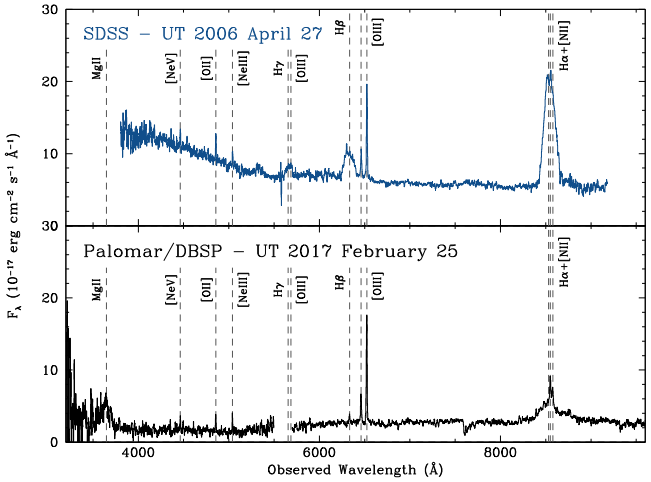

Figure 4. Multiepoch optical spectra of WISE J1052+1519. The top panel shows the SDSS spectrum from Spring 2006, while the lower panel shows the Palomar spectrum from Winter 2017. Key emission lines are labeled. In the past decade, the continuum has become significantly less blue, and higher order Balmer lines are no longer visible.

Palomar Observatory on UT 2017 January 30 (MJD = 57783). We obtained a single 900 s observation of the target using the 1.″5 slit at the parallactic angle. The night was photometric, though extremely windy, leading to highly variable seeing that exceeded 3″ (FWHM) at times. The poor seeing and image motion significantly compromised the quality of this spectroscopic observation. We processed the data using standard procedures and flux calibrated the spectrum with observations of the white dwarf spectrophotometric standard stars G191-B2B and HZ44 from Massey & Gronwall (1990) obtained on the same night. Though with a limited signal-to-noise ratio, the January data showed a spectrum with significantly less rest-frame UV/blue emission, and much weaker Balmer emission, suggesting a dramatic spectral change since the SDSS data from a decade earlier.

In order to improve the signal-to-noise ratio, we reobserved WISE J1052+1519 with DBSP on the Palomar 200″ on UT 2017 February 25 (MJD = 57809). We obtained two 600 s observations at the parallactic angle through the 1.″5 slit in photometric, good-seeing conditions. The February data were flux calibrated with observations of the spectrophotometric standards HZ14 and Feige 56 observed on that same night. Figure 4 presents the February Palomar data, which is of significantly better quality than the January Palomar spectrum.

Comparing the SDSS and Palomar spectra, we see that the source has faded significantly over the past decade. The rising blue continuum is no longer evident, nor are any of the broad Balmer emission lines other than Hα, which has faded by more than a factor of three. The Hα line has also become broader as the source faded, as expected. Specifically, the line width increases by a factor of ∼1.5–2 (depending on whether single or double Gaussian fits to the line are adopted), while the 5100 Å continuum fades by a factor of ∼2; using the Jun et al. (2015a) black hole mass estimator, we find consistent inferred black hole masses between the SDSS and Palomar spectra. Broad Mg II is visible in the Palomar data, but is blueward of the SDSS spectral range and thus is not available for direct investigation of temporal evolution. The narrow [O III] lines are slightly weaker in the Palomar data at the few tens of percent level. Since the narrow-line region of quasars are typically spatially extended on scales of tens to thousands of parsecs, this difference is likely due to the larger, 3″ diameter fiber used by SDSS compared to the 1.″5 wide slit used at Palomar.

From the SDSS spectrum, Shen et al. (2011) measure the Balmer emission lines to have full-widths at half-maximum of FWHM(Hα) = 5113 ± 129 km s^{-1} and FWHM(Hβ) = 5622 ± 145 km s^{-1}, and the 5100 Å continuum luminosity to be log$L$(5100)/(erg s^{-1}) = 44.107 ± 0.004. Shen et al. (2011) also reports the Hα line luminosity to be log L(Hα)/(erg s^{-1}) = 42.869 ± 0.015. Using the Jun et al. (2015a) black hole mass estimator based on FWHM(Hα) and L(5100), we derive a black hole mass for WISE J1052+1519 of $\log M_{\rm BH}/M_\odot$ = 8.61 ± 0.12. The Jun et al. (2015a) estimator based on FWHM (Hα) and L(Hα) implies a comparable black hole mass of $\log M_{\rm BH}/M_\odot$ = 8.66 ± 0.13. Adopting the bolometric correction of BC_{5100} = 9.26 from Shen et al. (2011), this implies the quasar had an Eddington ratio $\lambda_{\rm Edd}$ of 2% in the SDSS spectrum.

3.2. X-Ray Observations

Fortuitously, WISE J1052+1519 resides 40.′6 from the spiral galaxy MCG+03-28-022 (z = 0.022), which hosted the exceptionally luminous type II supernova SN 1988Z. At the time, it was the most distant and most luminous supernova detected at both radio (Van Dyk et al. 1993) and X-ray energies (Fabian & Terlevich 1996). This is presumably due to the supernova having exploded in a high-density environment, potentially associated with mass loss from its high-mass progenitor (Stathakis & Sadler 1991). WISE J1052+1519 was serendipitously detected in the 12.3 ks *ROSAT* follow-up X-ray observations of SN 1988Z obtained in 1995 May, and is listed as 2RXS J105203.9+151930 in the Second *ROSAT* All-Sky Survey (Boller et al. 2016). It is a ∼4σ detection, with a 0.1–2.4 keV flux of 1.3×10^{-12} erg cm^{-2} s^{-1} (assuming a power-law fit to the X-ray spectrum).

This relatively bright archival detection of our quasar prior to its optical fading inspired a successful *Swift* Target of Opportunity proposal to study how it has evolved at higher energies. *Swift* observed WISE J1052+1519 with the X-Ray Telescope (XRT; Burrows et al. 2005) and Ultraviolet/Optical Telescope (UVOT; Roming et al. 2005) instruments on UT 2017 February 17 (obsID 00034933001). We processed the raw data using the online analysis tools provided by the ASI Science Data Center[14] using HEAsoft version 6.20 and CALDB version 20111031. The total exposure was 4.3 ks with *Swift*/XRT, and 3.3 ks with *Swift*/UVOT (after coadding five separate frames taken with the UVM2 filter).

No X-ray source was detected at the coordinates of the *ROSAT* counterpart of WISE J1052+1519. The nearest detected source (SNR = 4.4) is ≈3.′5 offset at 10:51:50.46, +15:17:53.26, with a 0.3–10 keV count rate of $(6.0 \pm 1.4) \times 10^{-3}$ s^{-1}. Nearby 2σ detected sources have count rates $(1.3 \pm 0.7) \times 10^{-3}$ s^{-1} and $(1.6 \pm 0.8) \times 10^{-3}$ s^{-1}. We therefore estimate a 3σ upper limit on the count rate of W1052+1519 to be 3×10^{-3} s^{-1} in the 0.3–10 keV band. Assuming a simple unabsorbed power-law spectrum with a photon index Γ = 2, this corresponds to a flux limit of 1.07×10^{-13} erg cm^{-2} s^{-1} in the 0.3–10 keV band, and 4.90×10^{-14} erg cm^{-2} s^{-1} in the 2–10 keV band. Alternatively, for a softer Γ = 2.5 spectrum, the corresponding limits are 8.89×10^{-14} erg cm^{-2} s^{-1} and 2.30×10^{-14} erg cm^{-2} s^{-1}, respectively. This conversion to flux includes the Galactic column

[14] http://www.asdc.asi.it/mmia/index.php?mission=swiftmastr.

density, $N_{\rm H} = 2.3 \times 10^{20}$ cm^{-2} (Kalberla et al. 2005). The X-ray nondetection implies that WISE J1052+1519 has faded by at least an order of magnitude in the past two decades (Figure 2).

The target is detected at low significance ($\lesssim$5 sigma) in the *Swift*/UVOT UVM2 image at coordinates 10:52:03.5, +15:19:28.9. From aperture photometry using a 5 pixel (1.″8) radius, we estimate the source magnitude to be 21.2 ± 0.3 in the UVM2 filter ($\lambda_{\rm eff} = 2231$ Å). The background was determined from an annulus with an inner radius of 15 and outer radius of 30 pixels, including no other sources.

4. Physical Scenarios for Abrupt AGN Fading

We next discuss possible physical explanations for the extreme dimming observed for WISE J1052+1519, including testable predictions where possible. There are two broad categories of explanation for our observations: obscuration and changes to the inner disk.

4.1. Obscuration

4.1.1. Obscuration By a Cloud in a Keplerian Orbit

In principle, obscuration by a large cloud in a Keplerian orbit passing along our line of sight to WISE J1052+1519 provides a very simple and natural explanation for the observed quasar dimming, similar to what explains the strong (X-ray) variability of nearby changing-look AGNs such as NGC 1365 (e.g., Walton et al. 2014). This scenario, however, has several clear predictions, providing the potential to rule it out.

First, obscuration would imply that all wavelengths would dim essentially simultaneously, with the depth of the dimming in each waveband depending on the properties of the obscurer. A well-sampled multiwavelength light curve could test this model with sufficient data. Unfortunately, however, with only a handful of photometric points over a 10 year period in several key wavebands, the multiwavelength light curves of WISE J1052+1519 are too sparse to reliably determine whether or not there are lags between the various wavebands.

Second, an obscuring medium should have a strong wavelength dependence, with bluer photons being much more heavily extinguished than IR photons. For a standard $R_V = 3.1$ Fitzpatrick (1999) Milky Way reddening law, the extinction in U-band (rest-frame 3500 Å; observed ≈g-band for our source) is approximately 25 times higher than the extinction in L-band (rest-frame 3.5 μm; observed ≈$W2$ for our source); i.e., $A_U/E(B-V) \sim 4.3$ compared to $A_L/E(B-V) \sim 0.2$ (Schlafly & Finkbeiner 2011). This implies that the observed 1.8 mag g-band fading of WISE J1052+1519 should have been accompanied by negligible (<0.1 mag) fading in the mid-IR bands. This is significantly less than what we see in Figure 2.

Finally, as discussed in LaMassa et al. (2015) and Sheng et al. (2017), even with conservative assumptions, the crossing time for a cloud in a Keplerian orbit to occult the broad-line region would be a decade to several decades. This increases to well over a century to occult the inner regions of the mid-IR emitting dusty torus, which is the relevant emitting region for mid-IR selected changing-look quasars. This is substantially longer than the observed timescales, providing further strong evidence against obscuration by a cloud in a Keplerian orbit being the physical cause of the extreme variability in changing-look quasars.

We also briefly note that a cloud obscuring just the inner regions of the AGN accretion disk is an unlikely solution to explain the mid-IR variability. The mid-IR emission comes from a large, parsec-scale region, likely toroidal in nature, which reprocesses higher energy photons coming from the compact central engine, hundreds of astronomical units in scale. A cloud in a Keplerian orbit can easily occult that central region from the observers' line of sight, and, indeed, strong evidence of that has been seen at X-ray energies for some systems. Ignoring the challenges of the longevity of a cloud surviving interior to the dust sublimation radius, to cause mid-IR dimming, an implausibly large fraction of the sight lines between the central regions and the torus would need to be obscured. Furthermore, such an obscuring, large-scale cloud would be heated in the process, and become a new source of mid-IR thermal emission, thereby decreasing the level of observed mid-IR variability. These arguments all demonstrate that obscuration by a cloud in a Keplerian orbit is extremely unlikely as a physical scenario to explain changing-look quasars with strong mid-IR variability.

4.1.2. Obscuration By an Infalling Cloud

In order to bypass some of the challenges in terms of timescale and cloud size for obscuration by a dusty cloud in a Keplerian orbit, some authors have suggested that an infalling obscuring cloud provides a plausible alternative (e.g., Guo et al. 2016). However, there are multiple challenges to this scenario.

First, clouds typically will not be infalling, but instead will be in Keplerian orbits. In order to be infalling, the clouds need to lose their angular momentum. Though this could potentially occur in a collision with an approximately equal mass cloud of opposite angular momentum, such a collision would destroy the clouds, or, at least, leave something less coherent. Assuming the clouds survive, the freefall timescale $t_{\rm ff}$ for the cloud to infall from the dust sublimation radius $R_{\rm dust}$ (where we assume a typical dust composed of silicate and graphite grains; Mor & Netzer 2012),

$$R_{\rm dust} \approx 0.4 \text{ pc} \left(\frac{L_{\rm bol}}{10^{45} \text{ erg s}^{-1}}\right)^{1/2} \left(\frac{1500 \text{ K}}{T_{\rm sub}}\right)^{2.6}, \quad (1)$$

is given by

$$t_{\rm ff} \sim 100 \text{ years} \left(\frac{R}{0.4 \text{ pc}}\right)^{3/2} \left(\frac{M_{\rm BH}}{10^8 M_\odot}\right)^{-1}. \quad (2)$$

For typical cloud sizes $R_{\rm cloud}$ and overdensities $\delta_{\rm cloud} = \rho_{\rm cloud}/\rho_{\rm medium}$, this is comparable to the cloud-crushing time $t_{\rm cc}$, i.e., the timescale on which Kelvin–Helmholtz instabilities will shred the cloud into a fragmented, comet-like structure,

$$t_{\rm cc} \sim 100 \text{ years} \left(\frac{\delta_{\rm cloud}}{10^6}\right)^{1/2} \left(\frac{R_{\rm cloud}}{4 \times 10^{10} \text{ km}}\right) \left(\frac{v_{\rm rel}}{10^4 \text{ km s}^{-1}}\right)^{-1}, \quad (3)$$

where $v_{\rm rel}$ is the velocity of the cloud relative to the medium in which it is infalling (Klein et al. 1994). Though this calculation ignores the timescale on which the dusty, infalling, fragmenting cloud would be sublimated, this scenario suggests that an infalling, intact cloud would cause changes to the X-ray/UV spectrum on a timescale of several decades, not the month-scale

dramatic variability observed in the changing-look quasar SDSS J231742.60+000535.1 discussed by Guo et al. (2016). Furthermore, as noted earlier in the context of a Keplerian cloud obscuring the innermost regions of an AGN from the observer, this infalling scenario should not significantly affect the mid-IR luminosity of the AGN.

The arguments above emphasize the added value of mid-IR selection for identifying changing-look quasars. Namely, the large physical scale of the mid-IR emitting region combined with the longer wavelength baseline provided by mid-IR data together impose strong constraints for distinguishing intrinsic luminosity changes from obscuration. Having shown that obscuration is an unlikely cause of the changing-look quasars, particularly for mid-IR selected changing-look quasars such as WISE J1052+1519, we next consider changes to the innermost regions of the accretion disk as driving the observed fading.

4.2. Timescales for Changes to the Inner Disk

For possible explanations involving the accretion disk, we need estimates of the relevant timescales for processes at small radii (e.g., Czerny 2006). Four timescales are important to consider for our purposes: the orbital, thermal, cooling/heating front, and viscous timescales.

The orbital, or dynamical, timescale in the accretion disk is approximately $t_{\rm orb} \sim 1/\Omega$, where $\Omega = \sqrt{GM_{\rm BH}/R^3}$ is the Keplerian orbital angular frequency at radius R. This timescale is relevant for various processes, such as the timescale on which the disk achieves hydrostatic equilibrium, or the timescale on which magnetic loops with feet on the disk surface become entangled. The thermal timescale, corresponding to the timescale on which the disk heats or cools, is $t_{\rm th} \sim t_{\rm orb}/\alpha$, where α is the disk viscosity parameter (Shakura & Sunyaev 1973). Cooling and heating fronts propagate radially through an α disk at approximately the sound speed multiplied by the viscosity parameter, α (e.g., Hameury et al. 2009)—e.g., in the limit of $\alpha = 1$, the fronts propagate at the sound speed, while in less viscous disks (i.e., with smaller α), it becomes harder for the front to propogate. In the limit of $\alpha = 0$, there is no communication between neighboring annuli in the disk, so the fronts cannot propagate. Indeed, in such a situation, there is no accretion because there is no mechanism, like turbulence, to communicate between neighboring disk annuli and dissipate angular momentum. These heating and cooling fronts therefore cross the disk on timescales of $t_{\rm front} \sim (h/R)^{-1} t_{\rm th}$, where h/R is the disk aspect ratio, with $h = c_s/\Omega$ the disk height, and c_s is the local disk sound speed at radius R. Finally, the viscous disk timescale, the characteristic timescale of mass flow, is $t_\nu = (h/R)^{-2} t_{\rm th}$.

Using the parameters for WISE J1052+1519 derived at the end of Section 3.1 allows us assume a supermassive black hole with mass $M_{\rm BH} = 4 \times 10^8\, M_\odot$ and bolometric luminosity $L_{\rm bol} \sim 0.02\, L_{\rm Edd}$, where $L_{\rm Edd}$ is the Eddington luminosity and $\lambda_{\rm Edd}$ is the Eddington ratio, $\lambda_{\rm Edd} \equiv L_{\rm bol}/L_{\rm Edd}$. Then, the characteristic distance scale is the gravitational radius, $r_g = GM_{\rm BH}/c^2 \sim 5.9 \times 10^{11}$ m ($\sim$4 au). Assuming $L = \eta \dot{M} c^2$ is the luminosity due to accretion, where $\eta \sim 0.1$ is the luminosity efficiency of accretion, the characteristic mass-flow rate is

$$\dot{M} \approx 0.2\, M_\odot\ {\rm yr}^{-1} \left(\frac{\eta}{0.1}\right)^{-1} \left(\frac{M_{\rm BH}}{4 \times 10^8\, M_\odot}\right) \left(\frac{\lambda_{\rm Edd}}{0.02}\right). \quad (4)$$

Assuming a standard (relatively) thin-disk AGN model consisting of multiple annuli at temperatures that drop with radius, the mass-flow rate across each annulus is $\dot{M} = 3\pi\nu\Sigma$, where ν is the viscosity, Σ is the disk surface density, and the disk temperature drops as $T \propto R^{-3/4}$ (e.g., Zimmerman et al. 2005). The observed "photosphere" or surface of the disk has an effective temperature $T_{\rm eff}^4 \sim T^4/\tau$, where $\tau = \kappa\Sigma$ and κ is the opacity parameter. In order for the observed flux to drop dramatically at $\leqslant$3500 Å, the disk luminosity at $R < 150 r_g$ must drop significantly.

We can parameterize the relevant disk timescales for a black hole of mass $M_{\rm BH}$ at $R \sim 150 r_g$ as:

$$t_{\rm orb} \sim 10\ {\rm days} \left(\frac{M_{\rm BH}}{10^8\, M_\odot}\right) \left(\frac{R}{150 r_g}\right)^{3/2} \quad (5)$$

$$t_{\rm th} \sim 1\ {\rm year} \left(\frac{\alpha}{0.03}\right)^{-1} \left(\frac{M_{\rm BH}}{10^8\, M_\odot}\right) \left(\frac{R}{150 r_g}\right)^{3/2} \quad (6)$$

$$t_{\rm front} \sim 20\ {\rm years} \left(\frac{h/R}{0.05}\right)^{-1} \left(\frac{\alpha}{0.03}\right)^{-1} \left(\frac{M_{\rm BH}}{10^8\, M_\odot}\right) \left(\frac{R}{150 r_g}\right)^{3/2} \quad (7)$$

$$t_\nu \sim 400\ {\rm years} \left(\frac{h/R}{0.05}\right)^{-2} \left(\frac{\alpha}{0.03}\right)^{-1} \left(\frac{M_{\rm BH}}{10^8\, M_\odot}\right) \left(\frac{R}{150 r_g}\right)^{3/2}. \quad (8)$$

Since WISE J1052+1519 has a black hole mass of $M_{\rm BH} = 4 \times 10^8\, M_\odot$, these timescales range from $\sim$6 weeks to 1600 years for that source. Since we observe changes on timescales of a few years in this source, any changes in the disk are unlikely to be happening on the dynamical (i.e., orbital) timescale, which is far too short. Nor are they likely to be due to viscous effects or the propagation of cooling/heating fronts in the inner disk, which have characteristic timescales that are too long. In particular, the changing-look phenomenon might naturally have been assumed to be associated with the inner accretion disk clearing out, analogous to the disk truncation believed to be associated with state changes in Galactic binaries (e.g., Done et al. 2007; Neilsen et al. 2011). However, such disk truncation happens on the viscous timescale, which is orders of magnitude longer than the transitions observed in changing-look quasars. This rough parameterization above instead suggests that the thermal timescale most closely matches the observed source variability.

One caveat is that a revision of some of these parameters might make the heating/cooling front scenario plausible. The standard Shakura & Sunyaev (1973) thin disk assumes that once matter plunges across the innermost stable circular orbit (ISCO), which defines the inner edge of the accretion disk, the matter has no connection to the disk. This is called the zero-torque condition, and the disk remains thin all the way to the ISCO. If, instead, some connection is maintained between the plunging material and the innermost accretion disk, perhaps due to magnetic fields, the plunging material produces a torque in the inner accretion disk, causing it to heat up and inflate. Models and simulations both show that this is more likely than a zero-torque condition (e.g., Agol & Krolik 2000), meaning that $(h/R) \sim 0.2$ might be a more plausible value than the value of 0.05 assumed in Equation (4), at least, close to the

ISCO. Since this modification to the disk structure is due to a boundary condition at the ISCO, even in the inflated nonzero torque condition, the disk should be thin well before $150r_g$. Second, while numerical simulations (e.g., Hirose et al. 2009; Davis et al. 2010) tend to derive estimates for α consistent with the value assumed in Equation (4), King et al. (2007) argue that observations favor a typical range of $\alpha \sim 0.1$–0.4. They suggest that incomplete physics in the numerical simulations, including treatment of the global structure of the magnetic field, might cause the simulations to underestimate α. If we instead assume a more viscous disk with $\alpha \sim 0.3$, and further consider a region slightly closer to the black hole, $R \sim 100r_g$, then $t_{\rm front}$ drops by a factor of $\sim$80, becoming $\sim$1 year for WISE J1052+1519. Owing to its quadratic dependence on (h/R), the viscous timescale t_ν drops even more precipitously: it falls by a factor of $\sim$300, becoming $\sim$5.4 years. These timescales are consistent with the evolution observed in WISE J1052+1519 and many of the other changing-look quasars in the literature. Indeed, in our companion paper, Ross et al. (2018), we suggest that the observed spectral evolution in another mid-IR selected changing-look quasar is driven by a cooling front propagating outward, and then reflecting back inward as a heating front.

4.3. Causes of Changes in the Inner Disk

The discussion above shows that changes in the innermost disk occurring on the thermal or cooling/heating front timescale seem to be the most plausible explanation for the year-scale variability observed in changing-look quasars. We next consider potential triggers of these changes, which broadly can be broken into two classes: (i) disk instabilities, and (ii) local perturbations due to objects or events locally or elsewhere in the disk.

4.3.1. Disk Instabilities

Disk instabilities can occur for a variety of reasons and on a range of timescales (e.g., Lightman & Eardley 1974; Lightman & Shapiro 1976; Shakura & Sunyaev 1976). A classic, short timescale instability is due to an instability in $(\Sigma, T_{\rm eff})$ parameter space due to large changes in opacity from recombination as a result of small changes in Σ (e.g., Lin & Shields 1986). In this case, Σ changes locally so that the local disk lies on the unstable part of the $(\Sigma, T_{\rm eff})$ parameter space S-curve. Once this happens, $T_{\rm eff}$ can drop by an order of magnitude on approximately the thermal timescale $t_{\rm th}$ (or some small multiple thereof; Shakura & Sunyaev 1976). Since the midplane temperature T is approximately unchanged, but $T^4 = \tau T_{\rm eff}^4$, τ, the optical depth to the midplane, can increase dramatically. Recent work shows that this thermal instability seems to operate in simulations with turbulence driven by the magnetorotational instability (Jiang et al. 2014), though perhaps not in simulations that include realistic iron line opacities and sufficiently high metal abundances (Jiang et al. 2016).

In principle, another type of instability might cause the torque condition to change at the ISCO. Consider, for example, a quasar that starts in a nonzero torque state, and therefore with an inflated inner disk (e.g., Sirko & Goodman 2003). If some magnetohydrodynamical instability caused the torque to rapidly decrease, then the inner disk would cool and deflate, thereby creating a changing-look quasar. Ross et al. (2018) present an interesting source where our preferred explanation is exactly such a scenario.

4.3.2. Perturbations Due To Objects/Events

Changes in the inner disk state can also occur due to the presence of local perturbers, such as an extreme mass ratio inspiral (EMRI) event, or more distant changes in the accretion flow. A change in the local value of $\dot{\Sigma}$, which promotes instabilities in $(\Sigma, T_{\rm eff})$, such as those described above, might occur due to embedded supernovae in AGN disks (McKernan et al. 2014; McKernan et al. 2017), or stalling of objects migrating inward (Bellovary et al. 2016).

A large population of stellar-mass black holes, stellar remnants, and stars are expected in AGN disks (e.g., Syer et al. 1991; Artymowicz et al. 1993; McKernan et al. 2012). Torques from gas in the disk cause these secondary objects to migrate in the disk and a fraction of the secondaries will end up on the central supermassive black holes in an EMRI event. Once a secondary object ends up in the innermost regions of the accretion disk, its mass can become comparable to, or even dominate, the corotating disk mass. From Equation (4), a stellar-mass black hole of mass $\sim 10\,M_\odot$ could dominate the innermost gas flow on a timescale of decades. Therefore, the spectral output of the inner disk can change on the timescales of the EMRI. Specifically, initially migration torques on any embedded object in a disk whose mass is significantly less than the mass of the gas in the disk will cause the orbit to decay. The timescale of this orbital decay will range from tens of kyr to tens of Myr, depending on multiple factors, such as the starting point of the migration in the disk, the mass of the object, the disk surface density, and the disk aspect ratio. For all reasonable parameters, the timescale will be significantly larger than typical changing-look quasar timescales. Even once the migrating object has lost enough angular momentum from these migration torques and plunges to the central supermassive black hole, the relevant timescale becomes the freefall timescale (Equation (2)), which is an order of magnitude smaller than the changing-look quasar timescale. We are left with the most likely cause of the changing-look quasar phenomenon being some thermal or magnetic instability triggering a major change in the innermost accretion disk that then propagates on either the thermal or the heating/cooling front timescale.

5. Conclusions

We have presented WISE J1052+1519, one of the first mid-IR selected changing-look quasars reported thus far. The source was identified on the basis of its extreme variability in the *WISE*/NEOWISE data stream, having faded by more than a factor of two at 3.4 and 4.6 μm between 2010 and 2014. Optical surveys show comparable or greater fading over a slightly longer temporal baseline, while a comparison of archival *ROSAT* data from 1995 to Target of Opportunity *Swift* observations obtained in 2017 show the source has faded by at least a factor of 10 in the low-energy X-ray band. Motivated by this extreme fading, we obtained a second-epoch optical spectrum WISE J1052+1519 in early 2017 to compare with the archival SDSS spectrum from 2006. Over the intervening decade, the strong blue continuum has collapsed in this source, and most of the broad Balmer lines have disappeared; only broad Hα remains visible, albeit at a significantly weaker level.

We use this source as a touchstone to discuss physical models of abrupt quasar fading, a subject that has received considerable attention recently thanks to the growing ranks of wide-area ground-based optical surveys (e.g., LaMassa et al. 2015; Macleod et al. 2016; Ruan et al. 2016a, 2016b; Runnoe et al. 2016; Gezari et al. 2017; Sheng et al. 2017; Yang et al. 2018; Assef et al. 2018; Ross et al. 2018). In particular, we emphasize the unique value of multiepoch mid-IR photometry to test and exclude models that attempt to ascribe large changes in quasar luminosities to obscuration by an intervening cloud. The large, parsec-scale size of the mid-IR emitting region is too large to be extincted by an intervening cloud on the timescales probed thus far, and the long wavelength baseline of optical through mid-IR data provide a long lever arm with which to test if the observed variability is consistent with observed extinction laws.

Thus, when strong mid-IR variability is observed, the strong indication is that the changing-look phenomenon is not due to obscuration, but is rather due to changes in the innermost regions of the accretion disk, at distances $\lesssim 150\ r_g$ (i.e., $\lesssim 600$ au). We consider the range of relevant disk timescales at this distance, and show that the several week orbital, or dynamical timescale is far shorter than the typical changing-look quasar variability timescale of several years, while the millennium-long viscous timescale, which is the timescale on which the accretion disk can become truncated, is far too long. Importantly, these results show that the changing-look quasar phenomenon is physically distinct from related phenomenon seen more locally. Many changing-look Seyfert galaxies, at lower luminosity, are clearly associated with obscuration by an intervening cloud (e.g., NGC 1365; Risaliti et al. 2002; Rivers et al. 2015), while the state changes observed in Galactic binaries, i.e., systems with an accretion disk around a stellar-mass black hole or neutron star, appear to be associated with disk truncation (e.g., GRS 1915 +105; Neilsen et al. 2011).

We are instead left with the relevant timescale being the thermal timescale, or potentially the cooling/heating front timescale. We briefly discuss various physical phenomena that could cause abrupt changes in the temperature structure of the disk, such as (i) a rapid change in the torque at the ISCO radius, (ii) thermal disk instabilities where minor changes in the disk surface density can cause major opacity changes, and thus major temperature changes (e.g., Lightman & Eardley 1974; Lin & Shields 1986), and (iii) perturbations caused by an object or an event, such as an EMRI event.

In the coming years, the Zwicky Transient Facility (ZTF) and the Large Synoptic Survey Telescope (LSST), will begin providing deeper multiwavelength optical photometry with several-day cadence over large swaths of the sky. Many new changing-look quasars will be identified in these data streams. This will provide the exciting opportunity to find events while they are in process, rather than archivally. Unfortunately, these facilities will likely have minimal (ZTF) to zero (LSST) overlap with mid-IR survey missions such as *WISE* and *Spitzer*, but real-time discoveries will allow rapid follow-up and monitoring with both X-ray observations and optical/near-IR spectroscopy. Such data will be essential for disentangling which trigger or triggers cause the thermal changes observed in the inner accretion disks of changing-look quasars.

We thank the anonymous referee for a timely and informative report, which has improved our manuscript. We also thank Javier García for useful comments on the manuscript and Nikita Kamraj for assisting with the 2017 January Palomar observations. This publication makes use of data products from the *Wide-field Infrared Survey Explorer*, which is a joint project of the University of California, Los Angeles, and the Jet Propulsion Laboratory/California Institute of Technology, funded by the National Aeronautics and Space Administration. This publication makes use of data products from the Near-Earth Object Wide-field Infrared Survey Explorer (NEOWISE), which is a project of the Jet Propulsion Laboratory/California Institute of Technology. NEOWISE is funded by the National Aeronautics and Space Administration. C.R.T.S. was supported by the NSF grants AST-1313422, AST-1413600, and AST-1518308. D.S. acknowledges support from NASA through ADAP award 12-ADAP12-0109. B.M. and K.E.S.F. are supported by NSF PAARE AST-1153335, and with to thank JPL and Caltech for support during their sabbatical in early 2017. M.J.G., S.G.D., and A.J.D. acknowledge partial support from the NASA grant 16-ADAP16-0232, and NSF grants AST-1413600 and AST-1518308. N.P.R. acknowledges support from the STFC and the Ernest Rutherford Fellowship. A. M.M. acknowledges support from NASA through ADAP award NNH17AE75I. R.J.A. acknowledges support from FONDECYT grant number 1151408. M.B. gratefully acknowledges financial support from NASA Headquarters under the NASA Earth and Space Science Fellowship Program, grant NNX14AQ07H, and the support from the black hole Initiative at Harvard University, which is funded by a grant from the John Templeton Foundation. A.D.'s research was supported in part by the National Optical Astronomy Observatory (NOAO). NOAO is operated by the Association of Universities for Research in Astronomy (AURA), Inc. under a cooperative agreement with the National Science Foundation. H.D.J. acknowledges support from the Basic Science Research Program through the National Research Foundation of Korea (NRF), funded by the Ministry of Education (NRF-2017R1A6A3A04005158).

Facilities: SO:1.5 m, Blanco, Hale, PS1, Sloan, *WISE*.

ORCID iDs

Daniel Stern https://orcid.org/0000-0003-2686-9241
Matthew J. Graham https://orcid.org/0000-0002-3168-0139
Aaron M. Meisner https://orcid.org/0000-0002-1125-7384
Roberto J. Assef https://orcid.org/0000-0002-9508-3667
Arjun Dey https://orcid.org/0000-0002-4928-4003
S. G. Djorgovski https://orcid.org/0000-0002-0603-3087

References

Agol, E., & Krolik, J. H. 2000, ApJ, 528, 161
Arcavi, I., Gal-Yam, G., Sullivan, M., et al. 2014, ApJ, 793, 38
Artymowicz, P., Lin, D. N. C., & Wampler, E. J. 1993, ApJ, 409, 592
Assef, R. J., Kochanek, C. S., Brodwin, M., et al. 2010, ApJ, 713, 970
Assef, R. J., Prieto, J. L., Stern, D., et al. 2018b, ApJ, submitted (arXiv:1807.07985)
Assef, R. J., Stern, D., Kochanek, C. S., et al. 2013, ApJ, 772, 26
Assef, R. J., Stern, D., Noirot, G., et al. 2018a, ApJS, 234, 23
Becker, R. H., White, R. L., & Helfand, D. J. 1995, ApJ, 450, 559
Bellovary, J., Mac Low, M., McKernan, B., & Ford, K. E. S. 2016, ApJL, 819, L17
Blagorodnova, N., Gezari, S., Hung, T., et al. 2017, ApJ, 844, 46
Boller, T., Freyberg, M. J., Trümper, J., et al. 2016, A&A, 588, 103
Burrows, D. N., Hill, J. E., Nousek, J. A., et al. 2005, SSRv, 120, 165
Chambers, K. C., Magnier, E. A., Metcalfe, N., et al. 2016, arXiv:1612.05560

Czerny, B. 2006, in ASP Conf. Ser. 360, AGN Variability from X-Rays to Radio Waves, ed. I. M. McHardy, B. M. Peterson, & S. G. Sergeev (San Francisco, CA: ASP), 265
Davis, S. W., Stone, J. M., & Pessah, M. E. 2010, ApJ, 713, 52
Done, C., Gierliński, M., & Kubota, A. 2007, A&ARv, 15, 1
Drake, A. J., Djorgovski, S. G., Mahabal, A., et al. 2009, ApJ, 696, 870
Fabian, A. C., & Terlevich, R. 1996, MNRAS, 280, L5
Fitzpatrick, E. L. 1999, PASP, 111, 63
Gezari, S., Hung, T., Cenko, S. B., et al. 2017, ApJ, 835, 144
Goodrich, R. W. 1989, ApJ, 340, 190
Graham, M. J., Djorgovski, S. G., Drake, A. J., et al. 2017, MNRAS, 470, 4112
Graham, M. J., Djorgovski, S. G., Stern, D., et al. 2015a, Natur, 518, 74
Graham, M. J., Djorgovski, S. G., Stern, D., et al. 2015b, MNRAS, 453, 1562
Guo, H., Malkan, M. A., Gu, M., et al. 2016, ApJ, 826, 186
Hameury, J., Viallet, M., & Lasota, J. 2009, A&A, 496, 413
Hirose, S., Blaes, O., & Krolik, J. H. 2009, ApJ, 704, 781
Husemann, B., Urrutia, T., Tremblay, G. R., et al. 2016, A&A, 593, L9
Ichikawa, K., & Tazaki, R. 2017, ApJ, 844, 21
Jiang, Y., Davis, S. W., & Stone, J. M. 2014, ApJ, 796, 106
Jiang, Y., Davis, S. W., & Stone, J. M. 2016, ApJ, 827, 10
Jun, H. D., Im, M., Lee, H. M., et al. 2015a, ApJ, 806, 109
Jun, H. D., Stern, D., Graham, M. J., et al. 2015b, ApJL, 814, L12
Kalberla, P. M. W., Burton, W. B., Hartmann, D., et al. 2005, A&A, 440, 775
Kankare, E., Kotak, R., Mattila, S., et al. 2017, NatAs, 1, 865
King, A. R., Pringle, J. E., & Livio, M. 2007, MNRAS, 376, 1740
Klein, R. I., McKee, C. F., & Colella, P. 1994, ApJ, 420, 213
LaMassa, S. M., Cales, S., Moran, E. C., et al. 2015, ApJ, 800, 144
Lang, D. 2014, AJ, 147, 108
Lang, D., Hogg, D. W., & Schlegel, D. J. 2016, AJ, 151, 36
Lawrence, A., Bruce, A. G., MacLeod, C., et al. 2016, MNRAS, 463, 296
Lightman, A. P., & Eardley, D. M. 1974, ApJL, 187, L1
Lightman, A. P., & Shapiro, S. L. 1976, ApJ, 203, 701
Lin, D. N. C., & Shields, G. A. 1986, ApJ, 305, 28
Liu, T., Gezari, S., Heinis, S., et al. 2015, ApJ, 803, 16
Macleod, C. L., Ross, N. P., Lawrence, A., et al. 2016, MNRAS, 457, 389
Mainzer, A., Bauer, J., Grav, T., et al. 2014, ApJ, 784, 110
Massey, P., & Gronwall, C. 1990, ApJ, 358, 344
Matt, G., Guainazzi, M., & Maiolino, R. 2003, MNRAS, 342, 422
Matthews, T. A., & Sandage, A. R. 1963, ApJ, 138, 30
McElroy, R. E., Husemann, B., Croom, S. M., et al. 2016, A&A, 593, L8
McKernan, B., Ford, K. E. S., Bellovary, J., et al. 2017, MNRAS, submitted (arXiv:1702.07818)
McKernan, B., Ford, K. E. S., Kocsis, B., Lyra, W., & Winter, L. M. 2014, MNRAS, 441, 900
McKernan, B., Ford, K. E. S., Lyra, W., & Perets, H. B. 2012, MNRAS, 425, 460
Mor, R., & Netzer, H. 2012, MNRAS, 420, 526
Neilsen, J., Remillard, R. A., & Lee, J. C. 2011, ApJ, 737, 69
Rafiee, A., Pirkola, P., Hall, P. B., et al. 2016, MNRAS, 459, 2472
Ricci, C., Bauer, F. E., Arevalo, P., et al. 2016, ApJ, 820, 5
Risaliti, G., Elvis, M., & Nicastro, F. 2002, ApJ, 571, 234
Rivers, E., Risaliti, G., Walton, D. J., et al. 2015, ApJ, 804, 107
Roming, P. W. A., Kennedy, T. E., Mason, K. O., et al. 2005, SSRv, 120, 95
Ross, N. P., Ford, K. E., Graham, M. J., et al. 2018, MNRAS, in press (arXiv:1805.06921)
Ruan, J. J., Anderson, S. F., Cales, S. L., et al. 2016a, ApJ, 826, 188
Ruan, J. J., Anderson, S. F., Green, P. J., et al. 2016b, ApJ, 825, 137
Runnoe, J. C., Cales, S., Ruan, J. J., et al. 2016, MNRAS, 455, 1691
Schlafly, E. F., & Finkbeiner, D. 2011, ApJ, 737, 103
Shakura, N., & Sunyaev, R. A. 1973, A&A, 24, 337
Shakura, N., & Sunyaev, R. A. 1976, MNRAS, 175, 613
Shappee, B. J., Prieto, J. L., Grupe, D., et al. 2014, ApJ, 788, 48
Shen, Y., Richards, G. T., Strauss, M. A., et al. 2011, ApJS, 194, 45
Sheng, Z., Wang, T., Jiang, N., et al. 2017, ApJ, 846, 7
Sirko, E., & Goodman, J. 2003, MNRAS, 341, 501
Stathakis, R. A., & Sadler, E. M. 1991, MNRAS, 250, 786
Stern, D., Assef, R. J., Benford, D. J., et al. 2012, ApJ, 753, 30
Stern, D., Eisenhardt, P., Gorjian, V., et al. 2005, ApJ, 631, 163
Stern, D., Graham, M. J., Arav, N., et al. 2017, ApJ, 839, 106
Storchi-Bergmann, T., Eracleous, M., Livio, M., et al. 1995, ApJ, 443, 617
Syer, D., Clarke, C., & Rees, M. J. 1991, MNRAS, 250, 505
Tohline, J. E., & Osterbrock, D. E. 1976, ApJL, 210, L117
Urry, C. M., & Padovani, P. 1995, PASP, 107, 803
Van Dyk, S. D., Weiler, K. W., Sramek, R. A., & Panagia, N. 1993, ApJ, 419, 69
Walton, D. J., Risaliti, G., Harrison, F. A., et al. 2014, ApJ, 788, 76
Wright, E. L., Eisenhardt, P. R. M., Mainzer, A. K., et al. 2010, AJ, 140, 1868
Yang, Q., Wu, X., Fan, X., et al. 2018, ApJ, 862, 109
Zimmerman, E. R., Narayan, R., McClintock, J. E., & Miller, J. M. 2005, ApJ, 618, 832